Interband Transitions in Sn_xGe_{1-x} Alloys

Gang He and Harry A. Atwater

Thomas J. Watson Laboratory of Applied Physics, California Institute of Technology, Pasadena, California 91125

(Received 22 November 1996; revised manuscript received 21 May 1997)

Optical absorption measurements for diamond cubic Sn_xGe_{1-x} alloy films indicate strong interband transitions with a change in direct energy gap of $0.35 < E_g < 0.80$ eV for $0.15 > x > 0$. The optical energy gap undergoes an indirect to direct transition in this composition range and decreases much faster with Sn content than predicted by tight binding and pseudopotential calculations in the virtual crystal approximation. [S0031-9007(97)04003-9]

PACS numbers: 78.66.Li, 61.10.Kw, 78.20.Ci

Investigations of column IV semiconductor heterostructures have widened beyond Si_xGe_{1-x} alloys in order to broadly explore the possibilities for electronic structure manipulation in compounds which are isoelectronic with Si, such as Si_xC_{1-x} [1,2] alloys and Sn/Ge superlattices [3,4]. The Sn_xGe_{1-x} alloy system is one whose electronic structure has been a subject of interest and speculation for over a decade because of the tantalizing possibility of creating a column IV semiconductor with a tunable direct energy gap from constituent materials neither of which is a direct gap semiconductor. In this Letter, we demonstrate that an alloy of the semimetal cubic α-Sn and the indirect band gap semiconductor Ge produces a tunable direct energy gap semiconductor. Thus, this new semiconductor material is the only known example of a direct energy gap semiconductor among the compounds which can be formed from the column IV A elements (C, Si, Ge, Sn, and Pb). It is thus a new IV-IV semiconductor compound whose optical properties may broadly resemble those of III-V and II-VI compounds such as, e.g., $Hg_xCd_{1-x}Te$ and $Ga_yIn_{1-y}As_xSb_{1-x}$.

While Ge is characterized by an L point indirect fundamental energy gap, a direct energy gap lies 0.13 eV higher in energy owing to the conduction band minimum at the Γ point ($k = 0$). Tight-binding [5] and pseudopotential [6] electronic structure calculations in the virtual crystal approximation suggested that band mixing of the conduction band minima for Sn and Ge would lead to the onset of a direct fundamental energy gap in Sn_xGe_{1-x} alloys of approximately $0.55 > E_g > 0$ eV for $0.2 < x < 0.6$, but these electronic structure predictions have not been experimentally verified. Synthesis of Sn_xGe_{1-x} alloys is complicated by compositional metastability for $x > 0.005$, and thus nonequilibrium growth methods, such as molecular beam epitaxy, are required. Sn has a lower surface energy than Ge, and even molecular beam epitaxy is problematic owing to Sn surface segregation during growth. Nonetheless, growth of compositionally homogeneous semiconductor alloys is possible with Sn compositions in the range of $0 < x < 0.2$ [7], and growth of homogeneous alloy films up to $x = 0.34$ can be achieved by low energy ion-assisted molecular beam epitaxy [8]. However, no measurements of the optical constants and optical absorption have been made for Sn_xGe_{1-x} alloys, and thus little is known about the change in electronic structure with alloy composition.

To obtain information about the bulk solid structure and optical properties of cubic Sn_xGe_{1-x} alloys using thin film samples, strain-relieved compositionally homogeneous random alloys were investigated for films sufficiently thick so as to exclude the possibility of quantum carrier confinement-induced changes in optical absorption. Specifically, Sn_xGe_{1-x} alloys 50–300 nm in thickness were grown by molecular beam epitaxy at 180 °C on 10 nm thick relaxed Ge buffer layers (001)-oriented Si substrates. Ge epitaxial films were grown under the same conditions, except that the growth temperature was 450 °C. For each composition investigated, six samples of approximately 50, 100, 150, 200, 250, and 300 nm thickness were grown, with thickness and composition measured by Rutherford backscattering spectrometry and cross-sectional transmission electron microscopy.

Four Sn_xGe_{1-x} film structures were studied with $x =$ 0, 0.06, 0.11, and 0.15. Surface morphology was observed by *in situ* reflection high energy electron diffraction measurements, which indicated that the Sn_xGe_{1-x} films were epitaxial, and were rough on the monolayer scale, corroborated by postgrowth atomic force microscopy over 500 nm $\times$ 500 nm areas of the surface that indicated a root-mean-square roughness of 0.6 nm with maximum feature heights of 4 nm. The lateral compositional uniformity was found to be within $\pm 5\%$ relative composition over a 1 cm $\times$ 1 cm region on each sample, and each sample was compositionally uniform in depth, indicating negligible Sn segregation during growth. Cubic lattice parameters for the strain-relieved Sn_xGe_{1-x} alloys were inferred from the angular displacement of the (400) and (440) Cu K_α x-ray reflectivity of the film relative to the reflectivity of the Si substrate. The in-plane and out-of-plane lattice parameter measurements, shown on the left ordinate in Fig. 1, indicated that the films are fully relaxed (strain relieved) within experimental resolution, except for the $Sn_{0.06}Ge_{0.94}$ alloy which indicates a

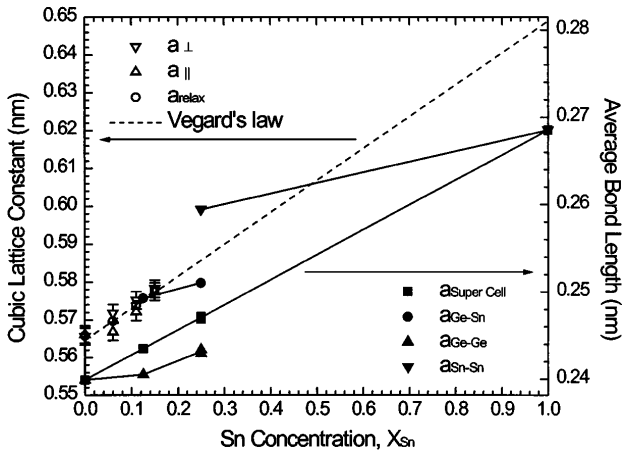

FIG. 1. Left ordinate: Sn_xGe_{1-x} alloy lattice parameters (measured by x-ray diffraction) as a function of Sn concentration x (measured by Rutherford backscattering): in-plane (open upright triangles) and perpendicular (open inverted triangles); calculated for fully strain-relieved films (open circles) from measured in-plane and perpendicular lattice parameters; calculation for virtual crystals (solid line). Right ordinate: the bond length as a function of Sn concentration calculated for the entire supercell (solid squares), for the average among Ge-Sn bonds (solid circles), for the average among Ge-Ge bonds (solid upright triangles), and for the Sn-Sn bonds (solid inverted triangles).

small but measurable residual strain. Moreover, we have also performed complementary local structural measurements using ^{119}Sn Mossbauer spectrometry and Raman spectroscopy, both of which indicate Sn incorporation into a substitutional diamond cubic alloy.

The dielectric function for Sn_xGe_{1-x} was obtained from thickness-dependent optical transmittance data [9]. The refractive index and the absorption coefficient for Sn_xGe_{1-x} and Ge films are shown in Figs. 2(a) and 2(b). Optical transmittance measurements were performed at 300 K for Sn_xGe_{1-x} films for the range of thicknesses and compositions indicated above with a Fourier transform spectrometer. An optical multilayer calculation was used to calculate the six transmittance spectra for each Sn composition by fitting to the real and imaginary parts of the dielectric function. The values for $n(\omega)$ and $k(\omega)$ were derived from an optical multilayer model that divides the sample into coherent substructures separated by incoherent layers. First an initial layer structure was assumed, and values for $n(\omega)$ and $k(\omega)$ were assumed for each layer. Then polarization density transfer matrices are calculated separately for each of these coherent substructures and incoherent layers, and are then combined to form the overall polarization transfer matrices from which optical transmission and reflection are calculated. The optical constants for the Sn_xGe_{1-x} layers were determined by iteratively fitting the experimentally measured thickness-dependent transmission spectra to the calculated optical transmission function at

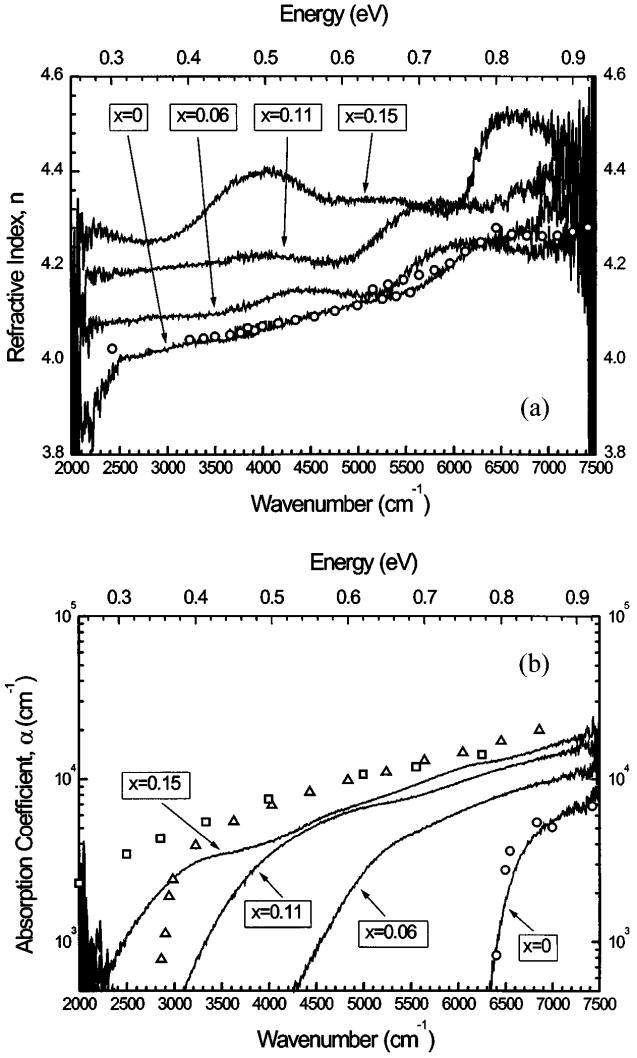

FIG. 2. Dielectric function and absorption data for Sn_xGe_{1-x} alloy films. In (a), refractive index; circle symbols refer to the tabulated Ge index (Ref. [11]). In (b), absorption coefficient for Sn_xGe_{1-x} alloy films; data points refer to Ge absorption (circles; Ref. [11]), InAs (triangles; Ref. [12]), and InSb (squares; Ref. [13]).

2000 points over 1000–9000 cm^{-1}, yielding a spectral resolution for the dielectric function of 4.71 cm^{-1}. The refractive index and extinction coefficient were varied independently at each wavelength so as to minimize the χ^2 error over each set of six transmittance spectra. The quality of the fit is illustrated by the very close agreement between measured values of $n(\omega)$ and $k(\omega)$ for Ge and accepted previously reported values [10]. The refractive index at 3000 cm^{-1} varies from $n = 4.0$ to $n = 4.3$ for $Sn_{0.15}Ge_{0.85}$, and the standard deviation in refractive index over the six measurements is $\sigma_n(\omega) < 0.05$ except for the $Sn_{0.15}Ge_{0.85}$ where $\sigma_n(\omega) = 0.1$ between 3000–4500 cm^{-1} and from 5800–6600 cm^{-1}. Noisy data in the refractive index and absorption spectra below 2500 cm^{-1} and above 7500 cm^{-1}, due to

multiphonon absorption in the silicon substrates and decreased instrumental efficiency, respectively, are not displayed in Figs. 2(a) and 2(b). The error analysis thus indicates that the resolution in refractive index is sufficient to indicate an increase as noted above, but that in the case of the $Sn_{0.15}Ge_{0.85}$ the relative maxima at 3800 and 6100 cm^{-1} may be measurement artifacts. The absorption data of Fig. 2(b) indicate a very rapid drop in the onset energy for absorption with increasing Sn content, with an absorption coefficient for all Sn_xGe_{1-x} compositions that is similar in magnitude to that seen for the onset of direct interband absorption in Ge at 0.8 eV. The absorption coefficients for Sn_xGe_{1-x} films are seen to be high and indeed comparable to the absorption coefficients across the direct energy gaps for InAs [11] and InSb [12] which are also plotted for reference in Fig. 2(b). Absorption data were analyzed using a model that includes contributions to absorption from the direct gap, the indirect gap, and a source of localized states characterized by an Urbach tail parameter. The values of these parameters are listed in Table I. Thus these data suggest that the $x = 0.15$ sample has a direct fundamental energy gap, and for the $x = 0.06$ and 0.11 samples, the difference in the direct and indirect energy gaps is smaller than the experimental error. The error is primarily in the measurement of the indirect energy gap, as absorption in submicron-thickness films constrains the minimum measurable extinction coefficient to approximately 0.01 and absorption coefficient to approximately 500 cm^{-1}. The presence of an Urbach tail may be attributable to the disorder arising from the approximately $10^7/cm^2$ dislocations present in the strain-relieved alloy layers.

The strong absorption features in Sn_xGe_{1-x} seen in Fig. 2(b) correspond to absorption across the direct energy gap of the alloy, and they establish an upper bound on the fundamental energy gap, given by the squares in Fig. 3. The errors in energy gap estimation resulting from compositional and strain inhomogeneities are given by the vertical error bars, and the compositional variation for each measurement is equal to the width of the square. A solid curve with linear and parabolic terms is fitted to the measured energy gap data. It is forced to an energy gap of -0.4 eV for Sn, and yields a bowing parameter of 2.8 eV. This bowing parameter is rather large compared to, e.g., the bowing parameter for Si_xGe_{1-x} of 0.206 eV [13]. Also shown as a dashed line in Fig. 3 is the direct energy gap variation predicted by tight-binding calculations [4]. Tight binding also predicts that the L point indirect energy gap ranges from 0.67 to 0.55 eV over the composition range $0 < x < 0.2$. The open triangle datum is an estimate of the energy gap of zinc blende $Sn_{0.5}Ge_{0.5}$ from a density functional theory calculation using the linear muffin tin orbital method [14]. Clearly there is a large discrepancy between the experimentally measured energy gap and any of the theoretical estimates which cannot be accounted for by sample strain or compositional inhomogeneities or measurement errors. The deviation between measurement and tight binding [5] or pseudopotential [6] calculations can be plausibly attributed to the large deviations in local structure from the virtual crystal approximation as discussed above. It is unclear why there is a large deviation of the measurements from the $Sn_{0.5}Ge_{0.5}$ (triangle) datum calculated by density functional theory, but there could be considerable error in the measurement-based estimate of the $Sn_{0.5}Ge_{0.5}$ energy gap due to extrapolation from measurements at lower Sn concentrations. Also, the calculation in Ref. [14] for zinc blende $Sn_{0.5}Ge_{0.5}$ employed added external potential corrections in the density functional theory calculations to reproduce the energy gaps of elemental Sn and Ge, and it is possible that these corrections may not be fully transferable to the zinc blende alloy.

In this work, cubic lattice parameter and local bond lengths and bond angles were calculated for Sn_xGe_{1-x} alloy structures in the range of the experimental compositions using density functional theory calculations in the local density approximation [15]. Norm-conserving pseudopotentials were used for Sn and Ge atoms, which were arranged in 8-atom supercells with periodic boundaries, with initial positions at lattice points of the cubic unit cell of the diamond lattice, and the minimum total energy unit cell volume was found. Wave functions were calculated self-consistently by conjugate gradient

TABLE I. Direct energy gap, indirect energy gap, and Urbach tail energy for Sn_xGe_{1-x} films derived from fit to absorption data in Fig. 2(b).

Absorption feature	Sn_xGe_{1-x} composition (x)	Energy (eV)
Direct gap	0.06	0.614 ± 0.004
Indirect gap	0.06	0.599 ± 0.019
Urbach tail	0.06	0.531 ± 0.004
Direct gap	0.11	0.445 ± 0.003
Indirect gap	0.11	0.428 ± 0.019
Urbach tail	0.11	0.383 ± 0.003
Direct gap	0.15	0.346 ± 0.003
Indirect gap	0.15	0.441 ± 0.004
Urbach tail	0.15	0.277 ± 0.007

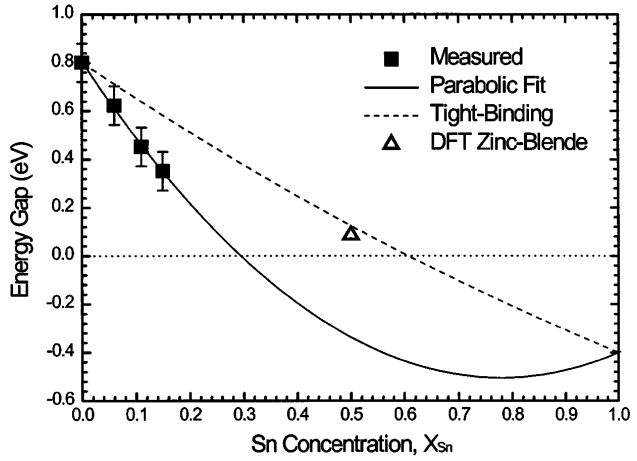

FIG. 3. Direct energy gap variation with Sn concentration: present measurements (squares), linear-parabolic fit to measurements (solid line), tight-binding calculation (dashed line), density functional theory calculation for zinc blende SnGe.

minimization, and local structure was evolved by atom movement via Feynman-Hellman forces to positions yielding minimum total energy, with an atomic position convergence criterion of 1 meV/nm. The plane basis cutoff energy was chosen to be 19.8 Ry, with a Brillouin zone integration cutoff length of 1 nm.

The three 8-atom Sn_xGe_{1-x} alloy supercell structures investigated consisted of a (i) Sn_1Ge_7 structure and two Sn_2Ge_6 structures, one of which has (ii) a Sn-Sn bond and the other which has (iii) no Sn-Sn bond in the supercell structure. The calculations indicate a small but positive alloy enthalpy of mixing relative to pure Sn and Ge of 12 meV/atom for the Sn_2Ge_6 with no Sn-Sn bond, 15 meV for the Sn_1Ge_7 structure, and 30 meV/atom for the Sn_2Ge_6 with a Sn-Sn bond. The calculated cubic lattice constants for Ge and Sn of 0.554 and 0.620 nm, respectively, are in good agreement with the measured low temperature values of 0.563 and 0.648 nm, for Ge and Sn, respectively. The calculated total energy as a function of unit cell volume yielded bulk elastic moduli of 77.6 and 53.1 GPa for pure Ge and Sn, which are in good agreement with the experimental values of 78 and 53 GPa for pure Ge and Sn, respectively. Bulk elastic moduli of 76.7 and 71.0 GPa were found for Sn_1Ge_7 and Sn_2Ge_6 structures, respectively. The calculated cubic lattice constants deduced from the energy-minimum unit cell volume are within 0.06% of the predictions resulting from the assumption of a virtual crystal of Sn_xGe_{1-x}. However, the averages for nearest-neighbor Ge-Ge, Sn-Sn, and Sn-Ge bonds in these alloy configurations show significant departures of bond length and bond angle from the virtual crystal approximation, as shown on the right abscissa of Fig. 1. The bond length deviations from the virtual crystal approximation are of the order of 5% of the bond length itself, and 40% of the bond length difference between Ge and Sn. Average Ge-Ge-Ge bond angles in Sn_1Ge_7 and Sn_2Ge_6 structures were, respectively, 110.7° and 116.5°.

These first experimental results on the optical properties of Sn_xGe_{1-x} alloy films are surprising, and are also very interesting from the perspective of fabrication of silicon-based optoelectronic devices with tunable absorption features or Ge/Sn_xGe_{1-x} heterojunctions because the Sn concentrations required to realize large changes in alloy energy gaps are much smaller than anticipated. Important questions also remain about the role of coherency strains of pseudomorphic epitaxial films in determining the optical properties of dislocation-free single crystals, which will be the subject of a subsequent report.

This work was supported by the National Science Foundation under Award No. DMR 95-03210.

[1] K. Brunner, K. Eberl, and W. Winter, Phys. Rev. Lett. **76**, 303 (1996).
[2] H. Rucker, M. Methfessel, E. Bugiel, and H. J. Osten, Phys. Rev. Lett. **72**, 3578 (1994).
[3] J. Olajos, P. Vogl, W. Wegscheider, and G. Abstreiter, Phys. Rev. Lett. **67**, 3164 (1991).
[4] W. Wegscheider, J. Olajos, U. Menczigar, W. Dondl, and G. Abstreiter, J. Cryst. Growth **123**, 75 (1992).
[5] D. W. Jenkins and J. D. Dow, Phys. Rev. B **36**, 7994 (1987).
[6] K. A. Mader, A. Baldereschi, and H. von Kanel, Solid State Commun. **69**, 1123 (1989).
[7] P. R. Pukite, A. Harwit, and S. S. Iyer, Appl. Phys. Lett. **52**, 2142 (1989); O. Gurdal, M-A. Hasan, M. R. Sardela, Jr., J. E. Greene, H. H. Radamson, J. E. Sundgren, and G. V. Hansson, Appl. Phys. Lett. **67**, 956 (1995).
[8] G. He and H. A. Atwater, Appl. Phys. Lett. **68**, 664 (1996).
[9] W. H. Brattain and H. B. Briggs, Phys. Rev. **75**, 1705 (1949).
[10] H. W. Icenogle, B. C. Platt, and W. L. Wolfe, Appl. Opt. **15**, 2348 (1976); H. B. Briggs, Phys. Rev. **77**, 287 (1950); R. F. Potter, Phys. Rev. **150**, 562 (1966); W. C. Dash and R. Newman, Phys. Rev. **99**, 1151 (1955).
[11] J. R. Dixon and J. M. Ellis, Phys. Rev. **123**, 1560 (1961).
[12] T. S. Moss, S. D. Smith, and T. D. F. Hawkins, Proc. Phys. Soc. London **70B**, 776 (1957).
[13] J. Weber and M. I. Alonso, Phys. Rev. B **40**, 5683 (1989).
[14] T. Brudevoll, D. S. Citrin, N. E. Christensen, and M. Cardona, Phys. Rev. B **48**, 17 128 (1993).
[15] M. C. Payne, M. P. Teter, D. C. Allan, T. A. Arias, and J. D. Joannopoulos, Rev. Mod. Phys. **64**, 1045 (1995); R. O. Jones and O. Gunnarsson, Rev. Mod. Phys. **61**, 689 (1989).